

Performance of Ag-Ag₂S core-shell nanoparticle-based random network reservoir computing device

Hadiyawarman^{1,2}, Yuki Usami^{1,2,*}, Takumi Kotooka¹, Saman Azhari^{1,2}, Masanori Eguchi^{3,4}, and Hirofumi Tanaka^{1,2,3,**}

¹ *Department of Human Intelligence Systems, Graduate School of Life Science and Systems Engineering, Kyushu Institute of Technology (Kyutech), 2-4 Hibikino, Wakamatsu, Kitakyushu 8080196, Japan*

² *Research Center for Neuromorphic AI Hardware, Kyushu Institute of Technology (Kyutech), 2-4 Hibikino, Wakamatsu, Kitakyushu 8080196, Japan*

³ *Fuzzy Logic System Institute, 1-5 Hibikino, Wakamatsu, Kitakyushu 8080135, Japan*

⁴ *National Institute of Technology, Kure College, Kure, Hiroshima 7378506, Japan*

E-mail address: usami@brain.kyutech.ac.jp*, tanaka@brain.kyutech.ac.jp**

Reservoir computing (RC), a low-power computational framework derived from recurrent neural networks, is suitable for temporal/sequential data processing. Here, we report the development of RC devices utilizing Ag-Ag₂S core-shell nanoparticles (NPs), synthesized by a simple wet chemical protocol, as the reservoir layer. We examined the NP-based reservoir layer for the required properties of RC hardware, such as echo state property, and then performed the benchmark tasks. Our study on NP-based reservoirs highlighted the importance of the dynamics between the NPs as indicated by the rich high dimensionality due to the echo state property. These dynamics affected the accuracy (up to 99%) of the target waveforms that were generated with a low number of readout channels. Our study demonstrates the great potential of Ag-Ag₂S NPs for the development of next-generation RC hardware.

1. Introduction

The computation performance (performance hereafter) of the von Neumann computer was greatly improved by miniaturizing the transistors and increasing the density according to Moore's Law.¹⁾ However, in recent years, the maximum permissible number of CPU transistors has remained constant, and further performance improvements have not been achieved to date. Although today's chip architecture is derived from some new approach, it is still deficient at solving more complex and nonlinear tasks, especially the computational tasks of artificial intelligence (AI), Big Data, and the Internet of Things (IoT). The limitation of the current von Neumann architecture lies in specific parts of parallel computation, and thus improvement requires a change in the solution paradigm to achieve higher computing performance.²⁾ Recently, several AI hardware systems are suggested for artificial neural network (ANN).³⁾⁻⁶⁾ Our previous work implied that reservoir computing (RC), a kind of the recurrent neural networks,⁷⁾⁻¹⁰⁾ might be one of the suitable candidates to replace the AI software system with the random network of nonlinear nanojunctions.^{3),11),12)}

To realize RC at the hardware level, an electrical component with analog electrical characteristics like synapses in the brain¹³⁾ is required. Memristor, a two-terminal passive component that exhibits nonlinear current-voltage characteristics with pinched hysteresis resulting from its charge-dependent resistance and memory characteristics, is considered an essential component to develop brain-mimicking hardware,¹⁴⁾⁻¹⁸⁾ especially in the RC architecture.¹⁹⁾⁻²²⁾ We can use the lower bias of the memristor switching, where the hysteresis is quite smaller than switching, to utilize the dynamic of the device much more effective for the RC devices because internal condition of the reservoir should be stable during the RC performed.

Chalcogenide compounds such as Ag₂S have been reported to exhibit memristive behavior²³⁾ and switching resulting from the redox reaction and ion migration inside the Ag/Ag₂S layer. Such kind of redox dynamics is expected as a good candidate of RC device²⁴⁾ and enabling them to successfully generate waveforms within an RC device architecture.²⁵⁾ However, quality of the nanowire network and number of junctions in the network affects the performance of the RC device even with a high number of readout channels. Like a human brain that consists of many synapse connections, to improve the performance, the number of memristors originating at the nodes that significantly influence network dynamics

must be increased by employing a material structure with a high surface area to volume ratio, such as nanoparticles. In our previous work, we successfully synthesized Ag-Ag₂S core-shell nanoparticles using a simple wet chemical reaction and characterized their structural properties and memristive behavior. Furthermore, we attempted to control the neuromorphic learning behavior with different pulse ratios.²⁶⁾ Our previous study also reported that the point of contact between the nanoparticles plays an important role in the performance of the memristor. Here, we report that the essential requirements for enabling RC devices such as nonlinearity, phase shift, and high harmonics generation (HHG), and then we demonstrate supervised learning by training the output weight to construct a specific target waveform and study their performance on the separation of signals.

2. Experimental methods

The experimental procedure is depicted in Fig. 1. In the first stage, the Ag-Ag₂S core-shell NPs were synthesized using the Brust–Schiffrin procedure according to previous works.^{14),28)} Structural properties such as particle dimension and chemical bonding at the surface of nanoparticles were previously determined by X-ray diffraction (XRD), transmission electron microscopy (TEM), and X-ray photoelectron spectroscopy (XPS).²⁶⁾ The resulting nanoparticles were core-shell structures with dimensions of a few tens of nanometers. The NPs were synthesized with an Ag/allyl mercaptan molar ratio of 0.25/1 because the resulting NPs were found to exhibit nonlinear and hysteresis features in the I - V curves, which are suitable for building RC devices.²⁶⁾ The synthesized NPs were then drop-casted onto lithographically pre-patterned SiO₂/Si substrates at 50 °C with Pt/Ti (24/6 nm) as the electrodes. The study on RC started by investigating the electrical characteristics of an HP 4156B semiconductor analyzer. Then, the dynamic properties of the reservoir layer, such as HHG and phase shift, were investigated by feeding the constant DC voltage and sine wave generated from the function generator (Hewlett Packard Model 33120A) to the device and recording the output from the multi-channels of the readout in the time-domain using a data acquisition system (National Instruments Model 9234). The output was then trained using a linear regression method to generate the target waveform. The accuracy and error were calculated for subsequent comparison with the performance of a nanowire-type Ag₂S reservoir²⁵⁾.

3. Results and discussion

A further cycle of bias injection to the device in the range of -5 to 5 V resulted in the hard switching phenomenon with a pinched hysteresis characteristic of a memristor (Fig. 2(a)), which is an important milestone in enabling the neuromorphic device, including RC.^{17),20)} The I–V characteristics of the NPs exhibited nonlinear and memristive behaviors with an on/off ratio of approximately 10^4 . In the RC device, the electrical property of the device must exhibit nonlinear mapping of the input signals into high-dimensional computational spaces while the synaptic weight of the input and the weight between the nodes in the reservoir layer are fixed. Therefore, by exhibiting the nonlinear I–V characteristics depicted in Fig. 2(a), the prepared device satisfied this RC device requirement.

To further understand the nonlinear transformation characteristics provided by the reservoir system, high dimensionality of the NP-based reservoir must be achieved. This property can be identified by analyzing the amplitude distribution in the frequency domain using the nonlinear technique of HHG. To this end, a bipolar sinusoidal wave with a peak amplitude of 1 V with a frequency of 10 Hz was applied to the device. The output current was then recorded, and the signal was converted by a fast Fourier transformation (FFT) process to obtain output amplitude characteristics in the frequency domain. As depicted in Fig. 2(b), at the input frequency of 10 Hz, the output current amplitude was observed at integer multiples of the input frequency; this behavior is indicative of hard switching from a high-resistance to a low-resistance state in an interconnected point-contact memristor that exceeds the percolation threshold.^{29),30)} Because the NP-based reservoir exhibited these two properties, nonlinear I–V characteristics and HHG, the NPs are considered strong candidates for RC devices. The characterized memristive device in an interconnected NP complex network was examined for emergent behaviors specific to its brain-like recurrent structure. Structurally, the network in the memristor-based RC is recurrent in that electrical signals and their feedback are produced simultaneously.

Another requirement for enabling RC is the phase shift that delays the output according to the RC formula described in Eqs. (1) and (2),³¹⁾⁾ where $X(t)$, w^{in} , $U(t)$, w , $X(t-1)$, $Y(t)$, and w^{out} are the current reservoir state, fixed input weight, input state, reservoir weight, past reservoir state, output state, and output weight, respectively. To investigate this delayed

output phenomena, Lissajous plots were analyzed for phase differences between the output voltage and a given input voltage.

$$\mathbf{X}(t) = \mathbf{f}\left(w^{\text{in}}\mathbf{U}(t) + w\mathbf{X}(t-1)\right) \quad (1)$$

$$\mathbf{Y}(t) = w^{\text{out}}\mathbf{X}(t) \quad (2)$$

The plots readily show the linear and non-linear relationships between the input and output voltages via amplitude and phase changes. [Figure 3](#) shows the Lissajous plots of the seven readouts from the NP-based device following the injection of a sinusoidal wave. It clearly shows that every output channel exhibited various phase differences between the input and the output, indicating delayed output. In terms of the shape of the Lissajous plot, the elliptical shape observed for the NP-based device is ideal as it indicates a complex network pathway that can create phase delays. Since one of the output signals, O_2 , showed a behavior of atomic switching, trajectory of each sweep overlapped which mean junctions through a path between input and O_2 electrodes keep original condition after every period. Thus, the NP-based system possessed the echo state property as governed by [Eqs. \(1\) and \(2\)](#). The state of the reservoir is dependent on the property of the input current and recent memory, and the echo state property is an important concept of RC at the critical point of fading memory.

The Ag-Ag₂S core-shell nanoparticles were then used to perform RC tasks as a hidden layer, as illustrated in [Fig. 1\(b\)](#), by injecting specific inputs and training the output weight through a supervised learning principle employing linear regression. First, a bipolar sinusoidal input bias with 1 V peak-amplitude with 10 Hz frequency was injected into one electrode. The output voltage from the rest of the electrode channels was recorded simultaneously using the LabVIEW program and used to construct various waveforms through the superposition of voltage outputs in the computation. The generated waveform r was then a weighted sum of the voltage outputs from the electrodes with the weights w_i calculated by linear regression:

$$r = \sum_{i=1}^n w_i V_i, \quad i = O_1, O_2, O_3 \dots \quad (3)$$

where V_i , n , i are the output electrode voltage, total number of outputs, and the labelled output number, respectively. Two parameters were used to quantify the performance of the reservoir: the accuracy and the differences between the generated and the target waveforms, which were respectively represented by the coefficient of determination (R^2) and the mean

square error (MSE), as expressed in the following equation:

$$MSE = \frac{\sum_{m=1}^P (y_{target}(t_m) - \sum_{i=1}^n w^i V^i(t_m))^2}{P} \quad (4)$$

$$R^2 = 1 - \frac{\sum_{i=1}^m (y_{reg} - y_{target})^2}{\sum_{i=1}^m (y_{reg} - y_{mean})^2} \quad (5),$$

where y_{reg} , y_{mean} , y_{target} is the output data, the mean of output, and the target waveform, respectively and w^i represents the weight coefficients to be trained with the maximum number of outputs at discrete time indices (t_m) over the total length (P). The results of the waveform generation tasks that were produced by applying linear regression to the outputs of 15 readout channels are depicted in Fig. 4, where the accuracy of each task is shown to assess the performance of the NP-based RC device. The highest accuracy was obtained when the waveform outputs were used to construct triangle and cosine waves due to the similarly shaped input and target waveforms, while the lowest accuracy was obtained in constructing square and sawtooth waves owing to the complex combination of odd and even harmonic waves. Even though the accuracy of both square and sawtooth waves was below 90% quantitatively, the generated wave was qualitatively close to the target waveform. The effect of the number of readout channels on the performance of waveform generation was then investigated by comparing various types of devices. As depicted in Fig. 5, the accuracy increased with an increase in the number of readout channels for all waveform types, supporting the use of numerous readout channels to optimize the training and suppress the error. Compared to the performance of the nanowire-based reservoir with 64 readout channels reported previously,²⁵⁾ only the accuracy for the trained sawtooth wave was slightly lower (< 90%), almost of all waveform generation task was improved accuracy even using much lower number of electrodes, indicating the importance of increasing the number of memristors junctions of the nanoparticle network to achieve better performance of the RC device.

4. Conclusions

We successfully fabricated an RC device utilizing Ag-Ag₂S NPs that were synthesized via simple experimental procedures at room temperature. The I–V characteristics of the NPs exhibited nonlinear and memristive behaviors with an on/off ratio of approximately 10⁴. The NP-based device exhibited rich HHG, indicating high dimensional mapping of the input.

Furthermore, the echo state property of the NP-based device was successfully demonstrated by the Lissajous plots in which a phase shift of all the readout channels was observed with various phase magnitudes. Because the NP-based device exhibited nonlinearity with HHG, a scale-free network, and echo state property, they were considered suitable for reservoir tasks. As a simple demonstration of RC, a supervised learning principle was applied to train the synaptic output weight to perform waveform generation tasks. The performance of the reservoir task was quantified by R^2 and MSE. RC with a multi-node device requires a certain number of readout channels to optimize the training. Furthermore, compared to nanowires, NP-based RC exhibits better performance with a smaller number of readout channels because the large surface area to volume ratio of the NPs increases the network dynamics, which can be achieved with a simple yet efficient synthesis protocol. We expect this novel approach for creating a brain-inspired computing device will provide a new perspective for developing future neuromorphic electronics based on the non-von Neumann computer architecture.

Acknowledgments

We thank Dr. K. Nakajima of the University of Tokyo and Prof. J. Gimzewski of UCLA for fruitful lectures and discussions on reservoir tasks. HT and YU would like to thank the Japan Society for the Promotion of Science for financial support (KAKENHI Nos. 15K12109, 19K22114, 20K21819, and 20K22485).

References

- 1) M. Hilbert and P. López, *Science* (80-.). **332** [6025], 60 (2011).
- 2) D. P. Rodgers, *Conf. Proc. - Annu. Symp. Comput. Archit.* 225 (1985).
- 3) S. K. Esser, P. A. Merolla, J. V. Arthur, A. S. Cassidy, R. Appuswamy, A. Andreopoulos, D. J. Berg, J. L. McKinstry, T. Melano, D. R. Barch, C. Di Nolfo, P. Datta, A. Amir, B. Taba, M. D. Flickner and D. S. Modha, *Proc. Natl. Acad. Sci. U. S. A.* **113** [41], 11441 (2016).
- 4) M. Davies, N. Srinivasa, T. H. Lin, G. Chinya, Y. Cao, S. H. Choday, G. Dimou, P. Joshi, N. Imam, S. Jain, Y. Liao, C. K. Lin, A. Lines, R. Liu, D. Mathaikutty, S. McCoy, A. Paul, J. Tse, G. Venkataramanan, Y. H. Weng, A. Wild, Y. Yang and H. Wang, *IEEE Micro* **38** [1], 82 (2018).
- 5) W. Wen, C. Wu, Y. Wang, K. Nixon, Q. Wu, M. Barnell, H. Li and Y. Chen, *Proc. - Des. Autom. Conf.* [DOI:10.1145/2897937.2897968].
- 6) C. Michaelis, A. B. Lehr and C. Tetzlaff, .
- 7) D. Verstraeten, B. Schrauwen and D. Stroobandt, *Proc. 16th Annu. ProRISC Work.* 454 (2005).
- 8) H. Jaeger and H. Haas, *Science* (80-.). **304** [5667], 78 (2004).

- 9) M. Lukoševičius and H. Jaeger, *Comput. Sci. Rev.* **3** [3], 127 (2009).
- 10) D. Verstraeten, B. Schrauwen, M. D'Haene and D. Stroobandt, *Neural Networks* **20** [3], 391 (2007).
- 11) J. Torrejon, M. Riou, F. A. Araujo, S. Tsunegi, G. Khalsa, D. Querlioz, P. Bortolotti, V. Cros, K. Yakushiji, A. Fukushima, H. Kubota, S. Yuasa, M. D. Stiles and J. Grollier, *Nature* **547** [7664], 428 (2017).
- 12) E. C. Demis, R. Aguilera, H. O. Sillin, K. Scharnhorst, E. J. Sandouk, M. Aono, A. Z. Stieg and J. K. Gimzewski, *Nanotechnology* **26** [20], 204003 (2015).
- 13) X. Yao, K. Klyukin, W. Lu, M. Onen, S. Ryu, D. Kim, N. Emond, I. Waluyo, A. Hunt, J. A. del Alamo, J. Li and B. Yildiz, *Nat. Commun.* **11** [1], 1 (2020).
- 14) T. Chang, S. H. Jo and W. Lu, *ACS Nano* **5** [9], 7669 (2011).
- 15) H. Y. Yoong, H. Wu, J. Zhao, H. Wang, R. Guo, J. Xiao, B. Zhang, P. Yang, S. J. Pennycook, N. Deng, X. Yan and J. Chen, *Adv. Funct. Mater.* **28** [50], 1 (2018).
- 16) L. Chua, *Nanotechnology* [DOI:10.1088/0957-4484/24/38/383001].
- 17) Hadiywarman, F. Budiman, D. G. O. Hernowo, R. R. Pandey and H. Tanaka, *Jpn. J. Appl. Phys.* [DOI:10.7567/JJAP.57.03EA06].
- 18) T. Hasegawa, T. Ohno, K. Terabe, T. Tsuruoka, T. Nakayama, J. K. Gimzewski and M. Aono, *Adv. Mater.* **22** [16], 1831 (2010).
- 19) T. Mazur, P. Zawal and K. Szaciłowski, *Nanoscale* **11** [3], 1080 (2019).
- 20) E. Wlazlak, M. Marzec, P. Zawal and K. Szaciłowski, *ACS Appl. Mater. Interfaces* **11** [18], 17009 (2019).
- 21) E. Wlazlak, P. Zawal and K. Szaciłowski, *ACS Appl. Electron. Mater.* **2** [2], 329 (2020).
- 22) L.-W. Chen, W. Wang, S. Ko, C.-Y. Chen, C. Hsu, F. Chiao, T. Chen, K. Wu and H. Lin, *Adv. Intell. Syst.* **2000196**, 2000196 (2020).
- 23) K. Terabe, T. Hasegawa, T. Nakayama and M. Aono, *Nature* **433** [7021], 47 (2005).
- 24) H. Tanaka, M. Akai-Kasaya, A. Termehyousefi, L. Hong, L. Fu, H. Tamukoh, D. Tanaka, T. Asai and T. Ogawa, *Nat. Commun.* **9** [1], 1 (2018).
- 25) E. C. Demis, R. Aguilera, K. Scharnhorst, M. Aono, A. Z. Stieg and J. K. Gimzewski, *Jpn. J. Appl. Phys.* [DOI:10.7567/JJAP.55.1102B2].
- 26) Hadiywarman, M. Eguchi and H. Tanaka, *Jpn. J. Appl. Phys.* [DOI:10.7567/1347-4065/ab5c77].
- 27) C. Battocchio, C. Meneghini, I. Fratoddi, I. Venditti, M. V. Russo, G. Aquilanti, C. Maurizio, F. Bondino, R. Matassa, M. Rossi, S. Mobilio and G. Polzonetti, *J. Phys. Chem. C* **116** [36], 19571 (2012).
- 28) H. Tanaka, T. Akai, D. Tanaka and T. Ogawa, *e-Journal Surf. Sci. Nanotechnol.* **12** [April], 185 (2014).
- 29) E. Nedaee Oskoe and M. Sahimi, *Phys. Rev. E - Stat. Nonlinear, Soft Matter Phys.* **83** [3], 1 (2011).
- 30) G. Z. Cohen, Y. V. Pershin and M. Di Ventra, *Appl. Phys. Lett.* **100** [13], 2012 (2012).
- 31) G. Tanaka, T. Yamane, J. B. Héroux, R. Nakane, N. Kanazawa, S. Takeda, H. Numata, D. Nakano and A. Hirose, *Neural Networks* **115**, 100 (2019).

Figure Captions

Fig. 1. (a) Illustration of reservoir computing (RC). (b) Schematic of the RC experiment using Ag-Ag₂S core-shell nanoparticles. The nanoparticles were used to increase the number of point-contact memristors, thereby improving the device dynamics and the performance of the RC hardware.

Fig. 2. (a) Input cycles ranging from -5 to 5 V resulted in hard switching with pinched hysteresis, indicating memristive behavior. Red arrow indicates a range, ± 1 V, where bipolar sinusoidal wave bias applied for tasks afterwards. This measurement was performed by two electrodes sample. (b) Output current in the frequency-domain following the injection of a bipolar sinusoidal wave with peak amplitude of 1 V with frequency of 10 Hz. High harmonic generation (HHG) was observed at integer multiples of the input frequency, indicating that the input nonlinearly mapped into high-dimensional space, which is suitable for building an RC device.

Fig. 3. Lissajous plots of output vs. input voltage from each readout channel. All the readout channels exhibited phase shifting, indicating that the output was delayed. Thus, the NP-based RC device possessed the echo state property.

Fig. 4. Demonstration of supervised learning through waveform generation of cosine (a), triangle (b), square (c), and sawtooth (d) as a target with 15 readout channels. The accuracy of shape-similar-waveforms (triangle and cosine) with the input sine wave was above 95%, while the accuracy of a more complex waveform (square and sawtooth) was below 90%. Although the generated sawtooth waveform exhibited the lowest accuracy, it was qualitatively closest to the target.

Fig. 5. Accuracy of the generated waveform against number of output channels. Increasing the number of output channels increased the accuracy and suppressed the mean-square-error. The highest efficiency ($\sim 99\%$) was achieved for the triangle wave with 15 output channels.

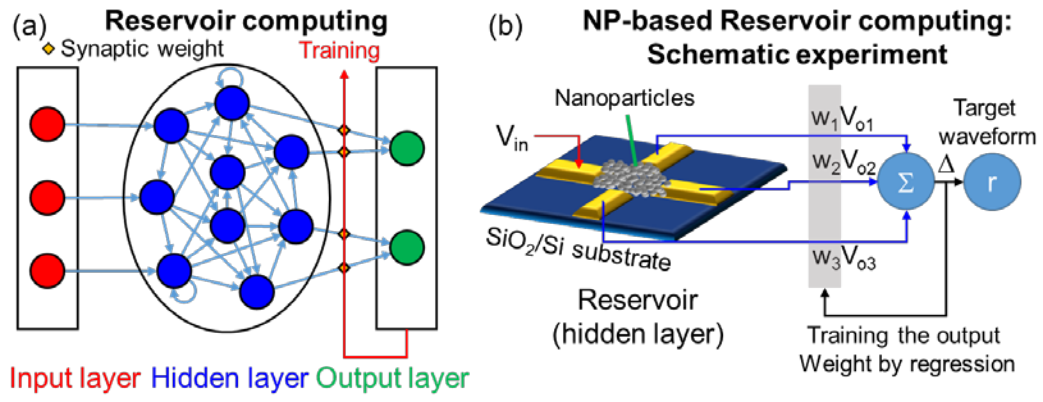


Fig. 1.

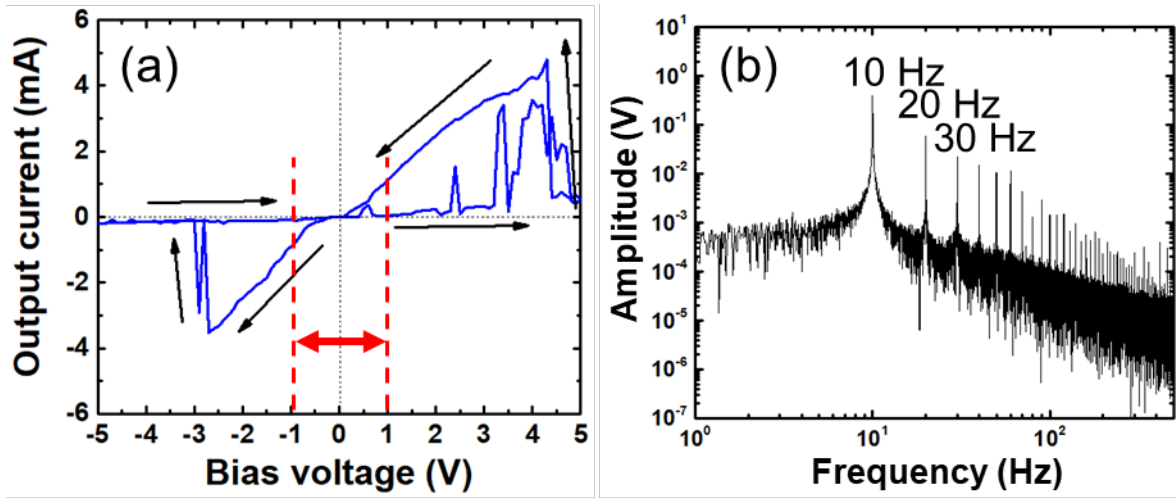


Fig. 2.

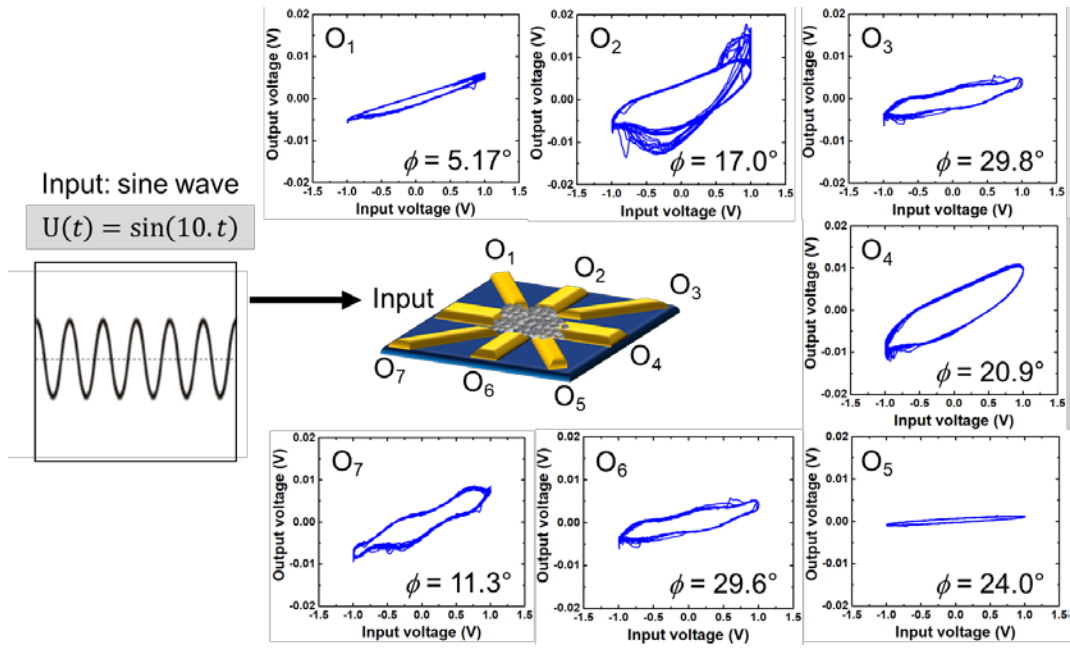


Fig. 3.

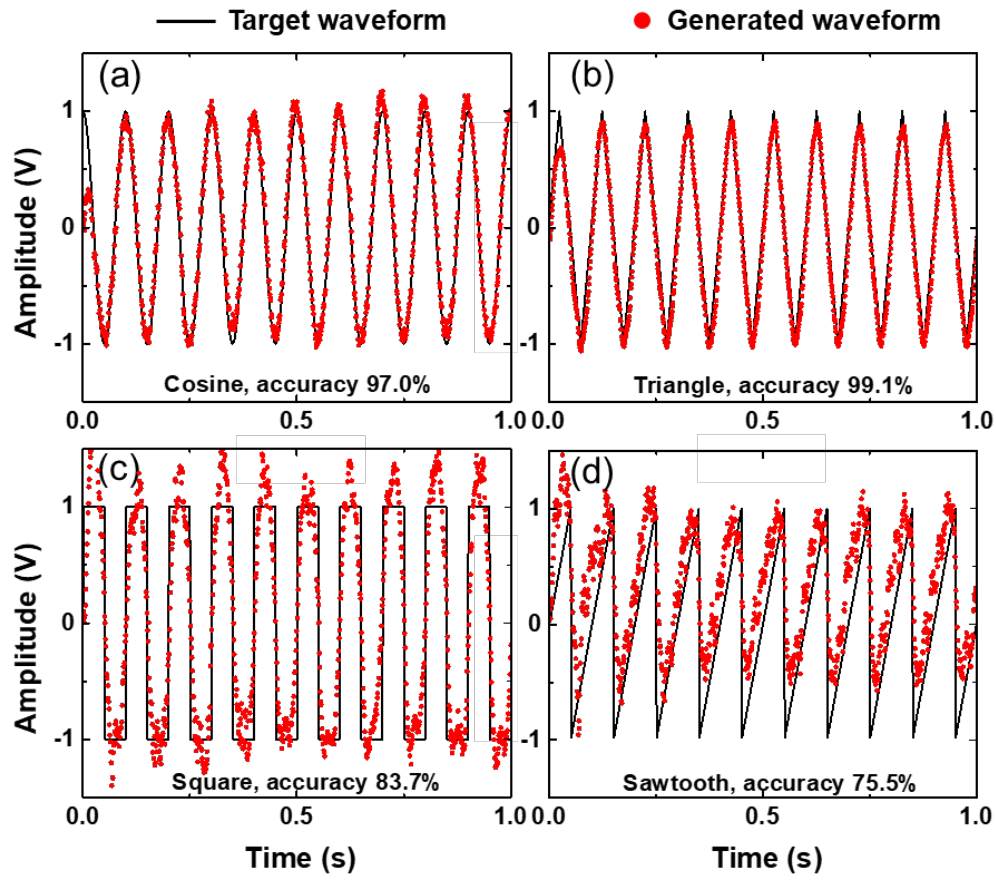


Fig. 4.

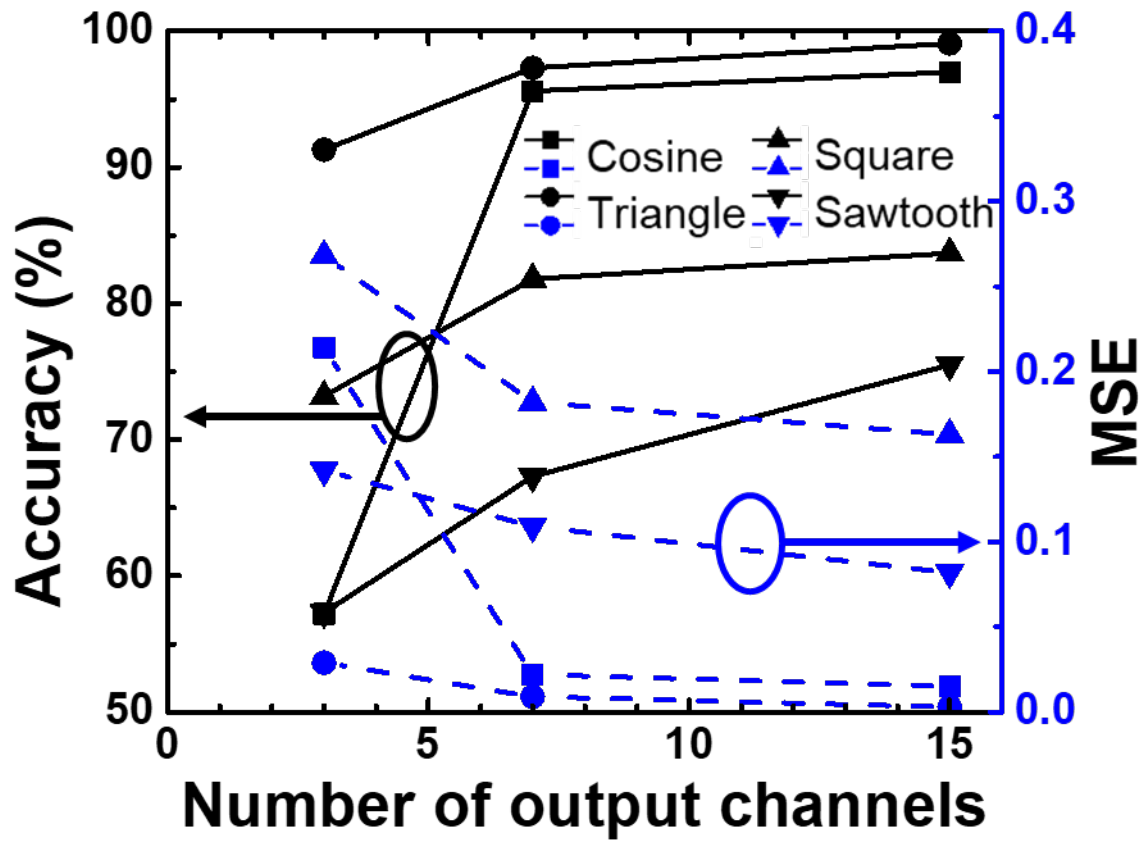


Fig. 5.